Inorg. Chem. **2003**, *42*, 689–695

Electronic Structure Contributions to Electron-Transfer Reactivity in Iron–Sulfur Active Sites: 2. Reduction Potentials

Pierre Kennepohl and Edward I. Solomon*

Department of Chemistry, Stanford University, Stanford, California 94305-5080

Received May 8, 2002

This study utilizes photoelectron spectroscopy (PES) combined with theoretical methods to determine the electronic structure contributions to the large reduction potential difference between $[FeCl_4]^{2-,1-}$ and $[Fe(SR)_4]^{2-,1-}$ ($\Delta E^0 \approx$ 1 V). Valence PES data confirm that this effect results from electronic structure differences because there is a similarly large shift in the onset of valence ionization between the two reduced species ($\Delta I_{vert} = 1.4 \pm 0.3$ eV). Specific electronic contributions to ΔI_{vert} have been investigated and defined. Ligand field effects, which are often considered to be of great importance, contribute very little to ΔI_{vert} ($\Delta E_{LF} < -0.05$ eV). By contrast, electronic relaxation, a factor that is often neglected in the analysis of chemical reactivity, strongly affects the valence ionization energies of both species. The larger electronic relaxation in the tetrathiolate allows it to more effectively stabilize the oxidized state and lowers its I_{vert} relative to that of the chloride ($\Delta E_{rlx} = 0.2$ eV). The largest contribution to the difference in redox potentials is the much lower effective charge (Z_{eff}^{Fe}) of the tetrathiolate in the reduced state, which results in a large difference in the energy of the Fe 3d manifold between the two redox couples ($\Delta E_{Fe\ 3d} =$ 1.2 eV). This difference derives from the significantly higher covalency of the iron–thiolate bond, which decreases Z_{eff}^{Fe} and significantly lowers its redox potential.

Introduction

Electron transfer (ET) is critical to biological systems and strict control of ET processes in vivo is extremely important for the proper functioning of most biochemical processes. Rubredoxins (Rds) are small globular metalloproteins that function as electron-transport agents in biology.[1,2] They are among the simplest of the known ET proteins and are good candidates for detailed investigations of their ET properties to determine the fundamental electronic structure contributions to their function. Specifically, our interests focus on defining and understanding the factors that control the thermodynamics (E^0) and kinetics (H_{DA} and λ_i) of electron transfer in $[Fe(SR)_4]^{2-,1-}$, the moiety that constitutes the active site of Rds.[2−5] This present paper specifically evaluates contributions to the reduction potentials of $[FeX_4]^{2-,1-}$ redox couples; issues relating to the kinetics of electron transfer in Rds are addressed in the following paper (part 3).[5]

Photoelectron spectroscopy (PES) is one of the direct methods for studying ionization (i.e., electron-transfer) processes. We have previously used variable-photon-energy PES studies of $[FeCl_4]^{2-,1-}$ to determine that dramatic electronic structure changes occur upon ionization of the reduced species; in particular, the oxidized state was found to have an inverted bonding scheme that can have a strong influence on the electron-transfer properties of this redox couple.[6−8] In the first paper in this series,[9] we extended these PES studies to quantitatively evaluate *electronic relaxation*, the change in the electronic wave function in response to oxidation, that occurs in $[FeCl_4]^{2-,1-}$ and $[Fe(SR)_4]^{2-,1-}$.

Specifically, the change in charge at the metal center due to electronic relaxation (Δq_{rlx}) was determined directly from the PES data. That study confirmed earlier qualitative conclusions that changes in the electronic structure are large

* Correspondence should be addressed to this author. Electronic-mail communication is encouraged (edward.solomon@stanford.edu).

(1) Spiro, T. G., Ed. *Iron−Sulfur Proteins*; Wiley-Interscience: New York, 1982; Vol. IV.
(2) Holm, R. H.; Kennepohl, P.; Solomon, E. I. *Chem. Rev.* **1996**, *96*, 2239−2314.
(3) Kennepohl, P.; Solomon, E. *I. J. Am. Chem. Soc.*, manuscript submitted.
(4) Kennepohl, P.; Solomon, E. I. *Inorg. Chem.*, manuscript submitted.
(5) Kennepohl, P.; Solomon, E. I. *Inorg. Chem.* **2003**, *42*, 696−708.
(6) Butcher, K. D.; Didziulis, S. V.; Briat, B.; Solomon, E. I. *Inorg. Chem.* **1990**, *29*, 1626−1637.
(7) Butcher, K. D.; Didziulis, S. V.; Briat, B.; Solomon, E. *I. J. Am. Chem. Soc.* **1990**, *112*, 2231−2242.
(8) Butcher, K. D.; Gebhard, M. S.; Solomon, E. I. *Inorg. Chem.* **1990**, *29*, 2067−2074.
(9) Kennepohl, P.; Solomon, E. I. *Inorg. Chem.* **2003**, *42*, 679−688.

10.1021/ic0203318 CCC: $25.00
Published on Web 01/16/2003

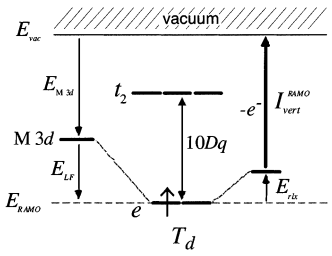

Figure 1. Contributions to the vertical ionization energy of the RAMO (I_{vert}^{RAMO}) in a transition metal complex. E_{M3d} depends on Z_{eff}^{M}, E_{LF} reflects the distorted T_d environment of the metal site, and E_{rlx} is the energetic effect of electronic relaxation.

in both of these redox couples[6,7] and further defined the nature of electronic relaxation in these systems as a ligand-to-metal transfer of charge to stabilize the oxidized metal center.[9] Additionally, Δq_{rlx} was found to be somewhat larger in $[Fe(SR)_4]^{2-,1-}$ than in the reference tetrachloride system. We now extend the analysis of valence and core PES data on these systems to assess the specific electronic structure contributions to their reduction potentials.

The reduction potentials of $[FeX_4]^{2-,1-}$ redox couples are quite sensitive to the nature of the ligands X. Of particular interest are the differences between $[FeCl_4]^{2-,1-}$ and $[Fe(SEt)_4]^{2-,1-}$; under the same experimental conditions, their redox potentials differ by almost 1 V.[10−12] Contributions to this potential difference can come from differences in their inherent electronic behavior as well as differential solvation effects in each oxidation state. Within the context of the Born equation, solvation differences will primarily result from differences in solvation radii. However, the small observed differences between the redox potentials of $[Fe(SEt)_4]^{2-,1-}$ and $[Fe(SCH_3)_4]^{2-,1-}$ ($\Delta E^0 \approx 0.1$) suggest more fundamental electronic differences between the thiolate and chloride redox species. Electronic contributions to the ionization process can be evaluated directly by comparison of the vertical ionization energies (I_{vert}) for the two reduced species. Such differences in I_{vert} provide a measure of the electronic contributions to adiabatic reduction potentials (E^0), which differ from the vertical ionization process by inclusion of the geometric changes that occur on ionization.

Frozen orbital contributions to the vertical ionization energy (I_{vert}) are defined as in Figure 1: the average energy of the metal 3d manifold ($E_{M\,3d}$) and the ligand field effect (E_{LF}) on the redox-active molecular orbital (RAMO).[2] This assumes that no change in the electronic structure occurs upon oxidation, i.e., that I_{vert}^{RAMO} is directly obtained from the energy of the RAMO (E_{RAMO}). The large amount of electronic relaxation in these systems (see part 1[9]) suggests that this assumption is unrealistic; changes in the electronic wave function will also affect the energy of the final state. This contribution is termed the electronic relaxation energy (E_{rlx}), and it must be included to complete the analysis. Each of the three above-mentioned contributions to I_{vert}^{RAMO} is evaluated independently. The overall importance of each of these electronic structure factors is further assessed in relation to the ET properties of the redox couples.

Experimental Section

The valence and core-level photoelectron spectroscopic (PES) data used in this paper are reported in part 1; experimental details are also provided there.[9] Aspects of the data are analyzed here to evaluate specific contributions to E^0. The PES spectra were simulated using a valence bond configuration interaction (VBCI) model, which is necessary to adequately describe shake-up satellite features in the spectra.[9] Full simulations, including the VBCI charge-transfer states as well as atomic multiplets, were calculated using the TT-Multiplets suite of computer codes provided by Dr. Frank M. F. de Groot.[13] All simulations were performed using an SGI Origin server.

Density functional theory (DFT) calculations were performed using the commercially available Amsterdam Density Functional (ADF1999 and ADF2000)[14−18] and Gaussian (Gaussian 98)[19] codes. In ADF, the Vosko, Wilk, and Nusair (VWN) local density approximation[20] was supplemented with standard nonlocal corrections from Becke[21] and Perdew[22,23] (BP86). All ADF results were obtained using a triple-ζ STO basis set (Basis IV) for the valence levels of all heavy atoms. Core levels were defined for the 1s and 2s/p orbitals of Fe and S and for the 1s orbitals of C, N, and O atoms. Complementary calculations using the BP86 functional were performed with Gaussian using a 6-311G(d,p) basis set. Results from the two quantum mechanics codes were similar. All calculations were performed on either an SGI Origin 2000 8-cpu R10k server running IRIX 6.5.3 or an Intel dual Pentium III Xeon system running RedHat Linux 7.0. Parallelization of ADF and Gaussian was done using built-in PVM and shared-memory architectures, respectively. Details of specific input parameters used for all published calculations are included as Supporting Information to this paper.

Results and Analysis

Valence VEPES data[9] for $[NEt_4]_2[FeCl_4]$ and $[NEt_4]_2[Fe(SPh)_4]$ are compared in Figure 2. Because the raw data have

(10) Hagen, K. S.; Watson, A. D.; Holm, R. H. *J. Am. Chem. Soc.* **1983**, *105*, 3905−3913.
(11) Maelia, L. E.; Millar, M.; Koch, S. A. *Inorg. Chem.* **1992**, *31*, 4594−4600.
(12) Koch, S. A.; Maelia, L. E.; Millar, M. *J. Am. Chem. Soc.* **1983**, *105*, 5944−5945.
(13) de Groot, F. M. F. *J. Electron Spectrosc. Relat. Phenom.* **1994**, *67*, 529−622.
(14) Baerends, E. J.; Ellis, D. E.; Ros, P. *Chem. Phys.* **1973**, *2*, 41−51.
(15) Versluis, L.; Ziegler, T. *J. Chem. Phys.* **1988**, *88*, 322−328.
(16) Te Velde, G.; Baerends, E. J. *J. Comput. Phys.* **1992**, *99*, 84−98.
(17) Guerra, C. F.; Snijders, J. G.; Te Velde, G.; Baerends, E. J. *Theor. Chem. Acc.* **1998**, *99*, 391−403.
(18) Te Velde, G.; Bickelhaupt, F. M.; Baerends, E. J.; Fonseca Guerra, C.; van Gisbergen, S. J. A.; Snijders, J. G.; Ziegler, T. *J. Comput. Chem.* **2001**, *22*, 931−967.
(19) Frisch, M. J.; Trucks, G. W.; Schlegel, H. B.; Scuseria, G. E.; Robb, M. A.; Cheeseman, J. R.; Zakrzewski, V. G.; Montgomery, J. A., Jr.; Stratmann, R. E.; Burant, J. C.; Dapprich, S.; Millam, J. M.; Daniels, A. D.; Kudin, K. N.; Strain, M. C.; Farkas, O.; Tomasi, J.; Barone, V.; Cossi, M.; Cammi, R.; Mennucci, B.; Pomelli, C.; Adamo, C.; Clifford, S.; Ochterski, J.; Petersson, G. A.; Ayala, P. Y.; Cui, Q.; Morokuma, K.; Malick, D. K.; Rabuck, A. D.; Raghavachari, K.; Foresman, J. B.; Cioslowski, J.; Ortiz, J. V.; Stefanov, B. B.; Liu, G.; Liashenko, A.; Piskorz, P.; Komaromi, I.; Gomperts, R.; Martin, R. L.; Fox, D. J.; Keith, T.; Al-Laham, M. A.; Peng, C. Y.; Nanayakkara, A.; Gonzalez, C.; Challacombe, M.; Gill, P. M. W.; Johnson, B. G.; Chen, W.; Wong, M. W.; Andres, J. L.; Head-Gordon, M.; Replogle, E. S.; Pople, J. A. *Gaussian 98*, revision A.lx; Gaussian, Inc.: Pittsburgh, PA, 1998.
(20) Vosko, S. H.; Wilk, L.; Nusair, M. *Can. J. Phys.* **1980**, *58*, 1200−1211.
(21) Becke, A. D. *Phys. Rev. A: Gen. Phys.* **1988**, *38*, 3098−3100.
(22) Perdew, J. P.; Burke, K.; Ernzerhof, M. *ACS Symp. Ser.* **1996**, *629*, 453−462.
(23) Perdew, J. P. *Phys. Rev. B: Condens. Matter* **1986**, *33*, 8822.

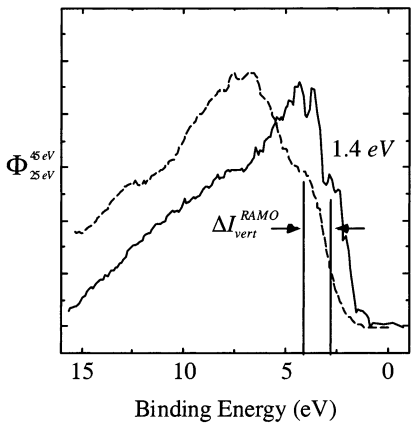

Figure 2. Valence $\Phi^{45\,eV}_{25\,eV}$ spectra for $[FeCl_4]^{2-}$ (− − −) and $[Fe(SPh)_4]^{2-}$ (—). The data are energy-referenced to deep-binding-energy peaks from the tetraethylammonium counterions in each of the species.

large contributions from counterions, $\Phi^{45\,eV}_{25\,eV}$ spectra (defined in part 1[9]) are used to enhance Fe 3d contributions to the spectra. The onset of ionization, given by the low-energy shoulder in both $\Phi^{45\,eV}_{25\,eV}$ spectra, is at much lower binding energy in the tetrathiolate complex. This onset energy corresponds with the lowest-energy vertical ionization energy (I^{RAMO}_{vert}) for oxidation of the reduced species, i.e., ionization of the redox-active molecular orbital (RAMO). The difference in I^{RAMO}_{vert} between $[FeCl_4]^{2-}$ and $[Fe(SPh)_4]^{2-}$ is large: $\Delta I^{RAMO}_{vert} = 1.4 \pm 0.3$ eV (see Figure 2). This large ΔI^{RAMO}_{vert} directly reflects electronic structure differences in the redox properties of the two species; the tetrathiolate complex is inherently easier to oxidize than its tetrachloride counterpart. This demonstrates that the observed ΔE^0 between $[FeCl_4]^{2-,1-}$ and $[Fe(SR)_4]^{2-,1-}$ is strongly related to differences in the inherent electronic behavior of the two redox couples.

I^{RAMO}_{vert} is considered as a sum of electronic structure contributions from the energy of the Fe 3d manifold ($E_{Fe\,3d}$), the effect of the ligand field (E_{LF}), and the electronic relaxation energy (E_{rlx}), as given in eq 1. The first two terms are positive (i.e., they increase I^{RAMO}_{vert}), whereas the last term acts to decrease the vertical ionization energy by stabilizing the final oxidized state.

$$I_{vert} = E_{Fe\,3d} + E_{LF} + E_{rIx} \quad (1)$$

When comparing the tetrathiolate complex to the tetrachloride reference system, differences between each of the pairs of terms ($\Delta E_{Fe\,3d}$, ΔE_{LF}, ΔE_{rlx}) become the meaningful quantities in determining the specific contributions to the large ΔI^{RAMO}_{vert} value observed from the experimental VE-PES data in Figure 2. Each of these factors is evaluated below.

Energy of the Fe 3d manifold ($\Delta E_{Fe\,3d}$). A direct experimental measurement of $\Delta E_{Fe\,3d}$ from valence PES data is not possible because ligand field and relaxation effects also contribute to valence ionization energies. However, $\Delta E_{Fe\,3d}$ derives from differences in the effective charges of the metal centers (Z^{Fe}_{eff}) in the two initial (ferrous) species. Such information can be derived from core ionization energies, which have been used extensively as a method of

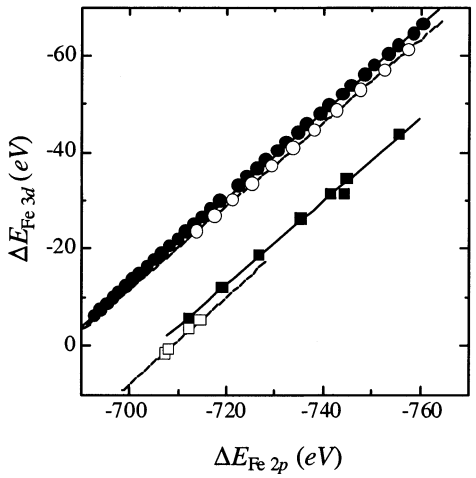

Figure 3. Relationship between Fe 2p and Fe 3d binding energies ($E_{Fe\,2p}$ vs $E_{Fe\,3p}$ in the ferrous complexes, circles) and ionization energies (ΔSCF for Fe 2p and Fe 3p ionization, squares) calculated using density functional methods. A range of effective nuclear charges (Z^{M}_{eff}) is obtained by evaluating the spherically symmetric Fe $3d^n$ atomic configuration for $0 < n < 8$. Calculations were performed for both the $M_S = 0$ (spin-restricted, solid circles and squares) and $M_S = 2$ (spin-unrestricted, open circles and squares) cases to determine the influence of spin polarization. Best-fit lines are shown for the spin-restricted (solid lines) and spin-unrestricted (dashed lines) cases; spin polarization has very little effect on the calculated LFER. The average value for the slope is 0.88 ± 0.04.

comparing charge density distributions in both organic[24−30] and inorganic[31] systems. There should therefore be a relationship between $E_{Fe\,3d}$ and the experimentally determined core $E_{Fe\,2p}$ binding energy of the unrelaxed final state.

Using DFT methods, we have evaluated the correlation between the ionization and binding energies of the Fe 2p and Fe 3d manifolds without complication from ligand field and other molecular effects. Using partial electron occupation of the Fe 3d manifold in an spherically symmetric field, Z^{Fe}_{eff} was modulated over a large range, and the theoretical behaviors of the Fe 2p and Fe 3d binding and ionization energies were tabulated. Figure 3 presents the relationship that exists between the core and valence initial-state binding energies, as well as the Fe 2p and Fe 3d ionization energies calculated using the ΔSCF method. In both cases, there is a near-linear relationship (slope ≈ 0.9) between the behaviors of the core and valence manifolds. It is therefore possible to estimate $\Delta E_{Fe\,3d}$ by experimentally obtaining $\Delta E_{Fe\,2p_{3/2}}$ and using the correlation obtained from Figure 3.

The Fe $2p_{3/2}$ core ionization data[9] are compared in Figure 4. There is an obviously large difference in the ionization energies of the two ferrous complexes: Fe $2p_{3/2}$ ionization is much easier for $[Fe(SPh)_4]^{2-}$ than for $[FeCl_4]^{2-}$, as the whole spectrum is shifted down in energy by >1 eV. In both cases, the data also show significant intensity in higher-

(24) Jolly, W. L.; Bomben, K. D.; Eyermann, C. J. *At. Data Nucl. Data Tables* **1984**, *31*, *433*- 493.
(25) Jolly, W. L. *J. Phys. Chem.* **1981**, *85*, 3792−3797.
(26) Jolly, W. L. *J. Phys. Chem.* **1981**, *85*, 3792−3797.
(27) Lee, T. H.; Jolly, W. L.; Bakke, A. A.; Weiss, R.; Verkade, J. G. *J. Am. Chem. Soc.* **1980**, *102*, 2631−2636.
(28) Jolly, W. L. *J. Phys. Chem.* **1986**, *90*, 6790−6793.
(29) Jolly, W. L.; Bakke, A. A. J. *Am. Chem. Soc.* **1976**, *98*, 6500−6504.
(30) Perry, W. B.; Jolly, W. L. *Inorg. Chem.* **1974**, *13*, 1211−1217.
(31) Lin, J.; Jones, P.; Guckert, J.; Solomon, E. I. *J. Am. Chem. Soc.* **1991**, *113*, 8312−8326.

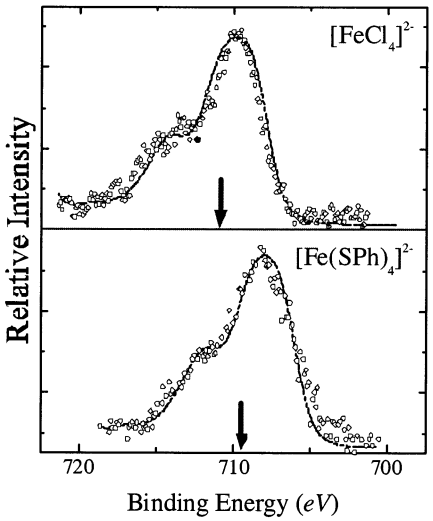

Figure 4. Core Fe $2p_{3/2}$, PES data for $[FeCl_4]^{2-}$ and $[Fe(SPh)_4]^{2-}$ referenced to the C 1s and N 1s peaks from the tetraethylammonium counterions in each complex. The dashed lines represent AM-VBCI simulations of the data as detailed in part 1.[9] The arrows indicate the relaxation-corrected Fe $2p_{3/2}$ binding energy ($E_{Fe\ 2p_{3/2}}$) in each species. The binding energy for $[FeCl_4]^{2-}$ (710.8 eV) is significantly deeper than that for $[Fe(SPh)_4]^{2-}$ (709.4 eV).

energy satellites as a result of electronic relaxation. To correct for relaxation effects, a VBCI model was used, the fundamentals of which are given in part 1.[9]

From this analysis, the relaxation-correction binding energy is simply the intensity-weighted average of the two component peaks in the data because the final-state intensity distribution is related to the unrelaxed final state through the application of the sudden approximation (arrows in Figure 4).[32] The energy of the unrelaxed final state (the Koopmans state, $\Psi_k{}^{\underline{M}}$) represents the binding energy for the Fe $2p_{3/2}$ orbital *without the effects of electronic relaxation.* Application of this methodology indicates that $[FeCl_4]^{2-}$ ($E_{Fe\ 2p_{3/2}} =$ 710.8 eV) is inherently more difficult to ionize than $[Fe(SPh)_4]^{2-}$ (709.4 eV) by 1.4 ± 0.4 eV. From Figure 3 (slope ≈ 0.9), this gives $\Delta E_{Fe\ 3d} \approx 1.2$ eV, indicating that differences in effective nuclear charge are a very significant contributor to the observed ΔI_{vert}^{RAMO} between $[FeCl_4]^{2-}$ and $[Fe(SPh)_4]^{2-}$.

Ligand Field Effects (ΔE_{LF}). The presence of a nonspherically symmetric ligand field modulates the valence ionization energy by altering the specific energy of the RAMO relative to the overall Fe 3d manifold determined above. The energetic contributions of such effects can be investigated using lower-energy bound-state spectroscopies. Detailed UV−vis and MCD studies of $[FeCl_4]^{2-}$ and $[Fe(SR)_4]^{2-}$ complexes have been performed and are reported in refs 33 and 34. From these studies, we construct the LF diagrams shown in Figure 5. Although $10Dq$ is greater in $[FeCl_4]^{2-}$, the overall effect of the ligand field on the doubly occupied Fe 3d orbital (the RAMO) of the high-spin d^6 configuration is greater in $[Fe(SR)_4]^{2-}$ because of a large

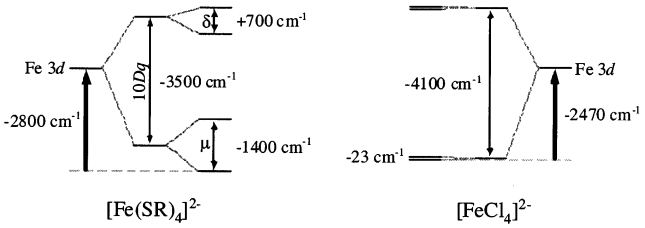

Figure 5. Ligand field splitting diagrams for $[Fe(SR)_4]^{2-}$ and $[FeCl_4]^{2-}$. These diagrams are constructed using the literature LF analysis in refs 33 and 34.

tetragonal distortion (μ) in the tetrathiolate. Within the context of this ligand field picture, the higher energy of the tetrachloride RAMO indicates that it should be slightly easier to oxidize than the tetrathiolate; from Figure 5, we estimate that $\Delta E_{LF} \approx -0.04$ eV. On the whole, this effect is very modest and *in the wrong direction* compared to ΔI_{vert}^{RAMO}. Therefore, the ligand field term, often used to discuss differences in E^0, is, in fact, not a significant contributor to the observed ΔI_{vert}^{RAMO} in these four-coordinate complexes.

Electronic Relaxation (ΔE_{rlx}). The last contribution to ΔI_{vert}^{RAMO} in eq 1 is from changes in the electronic wave function in response to the change in the molecular potential upon ionization. We have shown that electronic relaxation (quantified by the change in charge on the metal due to relaxation, Δq_{rlx}) is extremely large in $[FeX_4]^{2-}$ systems, and a VBCI model has been developed that defines a reference point, the Koopmans state, from which relaxation is determined.[9] The basic VBCI model developed in part 1 is extended here to calculate the difference in energy between the lowest-energy Koopmans ($\Psi_k{}^{\underline{M}}$) and final ($\Psi_k{}^{\underline{L}}$) states, which is the energy stabilization provided by electronic relaxation (E_{rlx} in Figure 6). E_{rlx} is obtained from eq 2 in terms of W_f and I_S/I_M, which are obtained directly from the experimental XPS data in Figure 4. W_f is the splitting between the two final states (the energy splitting between the main and satellite peaks in Figure 4), and I_S/I_M is the ratio of intensities between the two peaks in the experimental data.

$$E_{rlx} = W_f\left(\frac{I_S/I_M}{1 + (I_S/I_M)}\right) \qquad (2)$$

For valence ionization, E_{rlx} cannot be calculated directly from the data, but W_f and I_S/I_M can be derived from the VBCI parameters determined in part 1.[9] The model therefore allows the energetic effect of electronic relaxation for core and valence ionization of these species to be calculated; the results are given in Table 1. Electronic relaxation clearly has a very strong effect on the energetics of the ionization process. The effect is greater for core ionization, as expected because of the greater localization of the core hole. Furthermore, the energetic effect of electronic relaxation is greater in $[Fe(SR)_4]^{2-}$. This analysis allows for the calculation of ΔE_{rlx}; for valence ionization, E_{rlx} is greater in $[Fe(SR)_4]^{2-}$ by 0.17 eV (see Table 1).

The above model does not include the potentially significant influence of atomic multiplets (AMs).[13] It might be

(32) Manne, R.; Aberg, T. *Chem. Phys. Lett.* **1970**, *7*, 282−284.
(33) Briat, B.; Canit, J. C. *Mol. Phys.* **1983**, *48*, 33−61.
(34) Gebhard, M. S.; Koch, S. A.; Millar, M.; Devlin, F. J.; Stephens, P. J.; Solomon, E. I. *J. Am. Chem. Soc.* **1991**, *113*, 1640−1649.

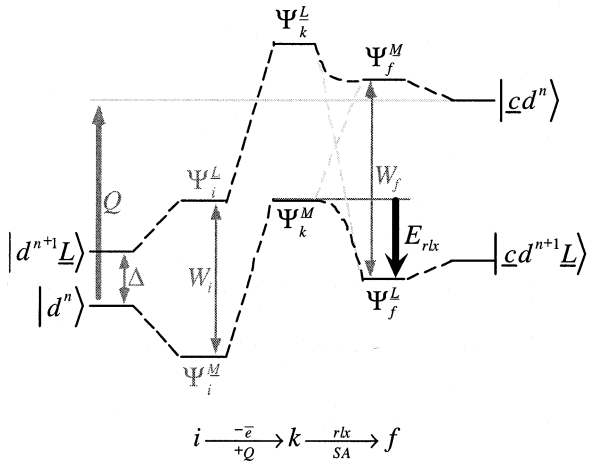

Δ = ΔE between metal (d^n) and CT ($d^{n+1}\underline{L}$)

T = covalent mixing parameter (not shown)

W_i = ground state charge transfer energy

Q = 2*p*-3*d* hole repulsion

U = 3*d*-3*d* hole repulsion (replaces Q in valence ionization)

W_f = final state charge transfer energy

E_{rlx} = electronic relaxation energy

Figure 6. VBCI model depicting a core ionization process. This diagram and the model that it represents are developed in part 1.[9] The stabilization energy obtained from electronic relaxation (E_{rlx}) is the difference in energy between $\Psi_k{}^{\underline{M}}$ and $\Psi_f{}^{\underline{L}}$.

Table 1. Relaxation Parameters Obtained from Application of the 1CT-VBCI Model to Core and Valence PES Data

	$E_{rlx}^{Fe\ 2p_{3/2}}$		$E_{rlx}^{Fe\ 3d}$	
complex	VBCI	+AM	VBCI	+AM
$[FeCl_4]^{2-}$	1.51	1.13	0.94	0.41
$[Fe(SR)_4]^{2-}$	1.65	1.27	1.11	0.63
ΔE_{rlx}	0.14	0.14	0.17	0.22

expected, a priori, that this problem should be more significant for valence ionization because the valence PES data cannot be properly simulated without inclusion of multiplet effects.[9] Furthermore, the exclusion of multiplets assumes that electronic relaxation is the same over all final states. The TT-Multiplets suite of programs[13] was used to address this issue by simulating both relaxed and unrelaxed ionization spectra in both systems. ΔE_{rlx} is the energy difference between the lowest-energy final states of the unrelaxed and relaxed spectra, as shown in Figure 7. The results from this AM-VBCI methodology are summarized in Table 1. The AM-VBCI results yield lower values for E_{rlx} in all cases but parallel the results obtained with the VBCI model. As expected, the absolute influence of the atomic multiplets is greater in the valence region, but the comparative results between $[FeCl_4]^{2-}$ and $[Fe(SR)_4]^{2-}$ remain the same: greater electronic relaxation during oxidation of $[Fe(SR)_4]^{2-}$ provides additional stabilization of the final state by 0.22 eV.

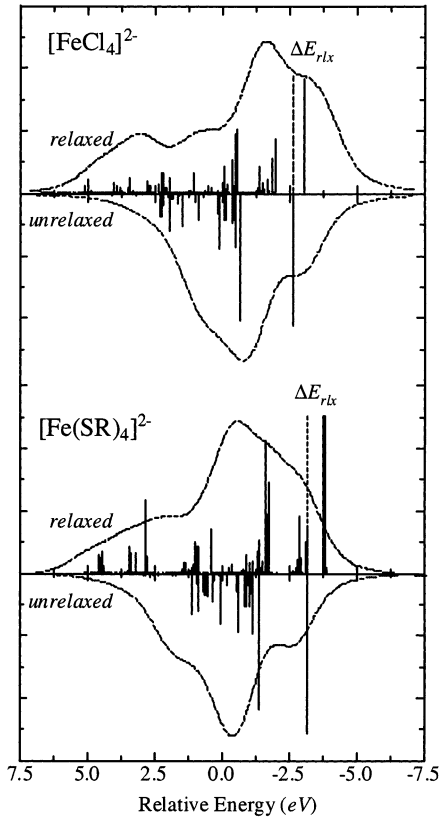

Figure 7. Valence PES AM-VBCI simulations for $[FeCl_4]^{2-}$ (top) and $[Fe(SPh)_4]^{2-}$ (bottom) including and excluding electronic relaxation. The simulations are performed using the VBCI parameters derived in part 1. Simulations for the unrelaxed spectra are performed by setting $U = 0$ and adjusting the energy of the ionization manifold relative to that of the relaxed simulations based on the sudden approximation.

Discussion

A combination of experiment and theory has provided a detailed understanding of the electronic structure differences that contribute to the thermodynamics of ionization in two $[FeX_4]^{2-}$ systems. It was determined that there is a large difference in the ionization potentials of $[FeCl_4]^{2-}$ and $[Fe(SR)_4]^{2-}$ ($\Delta I_{vert}^{RAMO} = 1.4$ eV) that is directly related to the experimental difference in their redox potentials ($\Delta E^0 \approx 1$ eV). ΔI_{vert}^{RAMO} provides an effective method of specifically evaluating the electronic structure factors that control the redox thermodynamics of the two redox couples. Our results indicate that the most significant difference between the two systems is their effective nuclear charges in the reduced state; the decreased positive charge on the metal in the tetrathiolate makes ionization easier by ~1.2 eV. The larger energy stabilization from electronic relaxation also contributes significantly (~0.2 eV), whereas ligand field effects are essentially negligible (<-0.05 eV).

The large difference in Z_{eff}^{M} results from the difference between the two complexes $[FeCl_4]^{2-}$ and $[Fe(SR)_4]^{2-}$ in the extent of covalency in the M−L bonds. PES data confirm that the ferrous tetrathiolate complex is significantly more

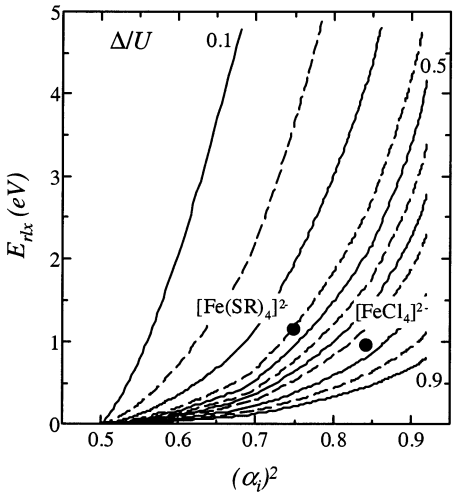

Figure 8. Relationship between covalency (α_i^2) and E_{rlx} from the VBCI analysis. The effect of Δ/U modulates the overall relationship between covalency and the relaxation energy similarly to that observed for the charge relaxation in Figure 5 of part 1. The calculated valence relaxations for $[FeCl_4]^{2-}$ and $[Fe(SPh)_4]^{2-}$ are given for comparison.

covalent, thus decreasing its Z_{eff}^{M} value relative to that of the tetrachloride. In our study on the kinetics of electron transfer (part 3), Z_{eff}^{M} was explicitly evaluated for each of the reduced species and found to be $0.15\bar{e}$ greater for $[FeCl_4]^{2-}$ than for $[Fe(SR)_4]^{2-}$.[5] The VBCI analysis for the ferrous species further indicates that the covalency differences result primarily from differences in the valence shell ionization energies (VSIEs) between the thiolate and chloride ligands.[35] The Δ value for $[Fe(SR)_4]^{2-}$ is much lower than that for $[FeCl_4]^{2-}$ because the ligand valence orbitals in the first species are higher in energy and thus much closer to the Fe 3d orbitals.

The analysis further demonstrates the influence of electronic relaxation on the redox properties in high-spin iron complexes. Although the energetic contribution to ΔI_{vert}^{RAMO} is small relative to the effect of Z_{eff}^{M}, electronic relaxation is still worth 0.2 V, which is not negligible. Furthermore, the absolute contributions of E_{rlx} to the vertical ionization energy are about 0.5 V (Table 1), which is clearly very significant. The greater E_{rlx} in $[Fe(SR)_4]^{2-}$ correlates with the larger charge redistribution upon relaxation (Δq_{rlx}), as determined in part 1.[9] This results from the more effective tetrathiolate LMCT pathways that stabilize the additional hole at the metal center upon oxidation. In part 1, we also detailed the electronic structure contributions to Δq_{rlx},[9] within the context of the VBCI model parameters (Δ, T, and Q) defined in Figure 6. A similar analysis is performed for E_{rlx}, and the general results are given in Figure 8. The relationship between the ground-state covalency of the site and E_{rlx} is somewhat more complex than that for Δq_{rlx}, but in general, the two relaxation parameters behave similarly following the same basic trends: as covalency and Δ/U increase, E_{rlx} decreases. Therefore, it is usually reasonable to consider that a large Δq_{rlx} value will result in a similarly large E_{rlx}.

(35) The VSIEs for atomic S and Cl are approximately 10.4 and 13.0 eV, respectively.

The small contribution from ligand field effects to the ionization processes is possibly somewhat surprising. Differences in redox potentials have often been attributed to differences observed in the ligand field splitting of transition metal complexes. In this case, however, the potential influence is tempered by the weak ligand field splitting that is inherent in near-tetrahedral complexes. The effect of ligand orientation at the active of Rds has been considered previously.[34,36] Our results confirm that changes in the ligand field have very little effect in modulating the redox potentials of the proteins.

Our goal has been to correlate the behavior of ΔI_{vert}^{RAMO} with differences in adiabatic redox potentials (ΔE^0). A direct comparison of ΔI_{vert}^{RAMO} and ΔE^0 is complicated by two factors that contribute solely to ΔE^0: (i) the differential solvation in the two oxidation states and (ii) the geometric changes that accompany the adiabatic oxidation process. Solvation effects depend strongly on the nature of the solvent itself and are not considered in this study. The geometric changes are intrinsic to the systems under study; thus, we can evaluate the influence of geometric changes upon ionization, an issue that is addressed explicitly in the complementary kinetics study (part 3).[5] There is a large difference between $[FeCl_4]^{2-}$ and $[Fe(SR)_4]^{2-}$ in geometry change upon oxidation. The M−L bond distances in the tetrachloride complex shorten by over 0.1 Å, whereas those in $[Fe(SR)_4]^{2-}$ change by only ~0.05 Å. In part 3, the potential energy surfaces of the two redox couples are evaluated using DFT methods.[5] An adiabatic correction to the ionization process can be estimated from these surfaces; the correction is calculated to be larger for $[FeCl_4]^{2-}$ (0.3 eV) than for $[Fe(SR)_4]^{2-}$ (0.1 eV).[37] The adiabatic correction decreases the difference between the ionization energies of the two redox couples, yielding $\Delta I_{adiabatic}^{RAMO} \approx 1.2$ eV. This result correlates well with the reduction potential difference of approximately 1 V.

This present study, aimed at determining the electronic structure contributions to redox potential differences between $[FeCl_4]^{2-}$ and $[Fe(SR)_4]^{2-}$ complexes, has provided key insights into the inherent electronic factors that contribute to redox thermodynamics. For these systems, we find that the effective charge of the metal center is the key contributor to the large difference in valence ionization energies in the two systems; Z_{eff}^{M} is significantly lower for $[Fe(SR)_4]^{2-}$, making this species easier to oxidize by >1 eV. This difference derives from the higher covalency of the tetrathiolate, which preferably stabilizes the oxidized state. By contrast, ligand field effects play a negligible role in modulating the redox potentials of these four-coordinate systems. Electronic relaxation also modulates the ionization energy considerably and should be considered in the investigation of reduction potentials of transition metal systems.

(36) Koemer, J. B.; Ichiye, T. *J. Phys. Chem. B* **1997**, *101*, 3633−3643.
(37) The adiabatic correction is the calculated energy difference between the oxidized structure at the two (reduced and oxidized) optimized geometries.

Acknowledgment. Financial support for this research was provided by the National Research Foundation (NSF CHE-9980549). Valence PES data were obtained at the Stanford Synchrotron Radiation Laboratory (SSRL). SSRL is funded by the U.S. Department of Energy, Office of Basic Energy Sciences. Partial financial support was provided to P.K. from SSRL. Graduate fellowship support for P.K. was provided by the Natural Sciences and Engineering Research Council of Canada (NSERC/CRSNG).

Supporting Information Available: Input files and structural information for DFT calculations used in this paper. Input files for TT-Multiplets simulations. This material is available free of charge via the Internet at http://pubs.acs.org.

IC0203318